Real-time coherent detection of phase modulated ultrashort pulses after time-to-space conversion and spatial demultiplexing

Dror Shayovitz,[1,*]Harald Herrmann,[2] Wolfgang Sohler,[2]Raimund Ricken,[2] Christine Silberhorn,[2] and Dan M. Marom[1]

[1]*Department of Applied Physics, Hebrew University of Jerusalem, Jerusalem, 91904, Israel*
[2]*Department of Applied Physics, The University of Paderborn, Warburger Str. 100 D-33098, Paderborn, Germany*
*dror.shayovitz@mail.huji.ac.il

Abstract: Phase modulated sub-picosecond pulses are converted by a time-to-space processor to quasi-monochromatic spatial beams that are spatially demultiplexed and coherently detected in real-time. The time-to-space processor, based on sum-frequency generation (SFG), serves as a serial-to-parallel converter, reducing the temporal bandwidth of the ultrashort pulse to match the bandwidth of optoelectronic receivers. As the SFG process is phase preserving, we demonstrate homodyne coherent detection of phase modulated temporal pulses by mixing the demultiplexed SFG beam with a narrow linewidth local oscillator (LO) resulting in single-shot phase detection of the converted pulses at a balanced detector. Positively and negatively phase-modulated signal pulses are individually detected and LO shot noise limited operation is achieved. This demonstration of real-time demultiplexing followed by single-shot full-field detection of individual pulses, highlights the potential of time-to-space conversion for ultrahigh bit rate optical communications and data processing applications.

OCIS codes: (320.0320) Ultrafast optics; (190.0190) Nonlinear optics.

References and links

1. R. Essiambre and R. W. Tkach, "Capacity trends and limits of optical communications networks," Proc. IEEE **100**(5), 1035–1055 (2012).
2. E. M. Ip and J. M. Kahn, "Fiber Impairment Compensation Using Coherent Detection and Digital Signal Processing," J. Lightwave Technol. **28**(4), 502–519 (2010).
3. H. Weber, R. Ludwig, S. Ferber, C. Schmidt-Langhorst, M. Kroh, V. Marembert, C. Boerner, and C. Schubert, "Ultrahigh-Speed OTDM-Transmission Technology," J. Lightwave Technol. **24**(12), 4616–4627 (2006).
4. J. P. Sokoloff, P. R. Prucnal, I. Glesk, and M. Kane, "A Terahertz Optical Asymmetric Demultiplexer (TOAD)," IEEE Photon. Technol. Lett. **5**(7), 787–790 (1993).
5. H. Sotobayashi, C. Sawaguchi, Y. Koyamada, and W. Chujo, "Ultrafast walk-off-free nonlinear optical loop mirror by a simplified configuration for 320-Gbit / s time-division multiplexing signal demultiplexing," Opt. Lett. **27**(17), 1555–1557 (2002).
6. K. I. Kang, I. Glesk, T. G. Chang, P. R. Prucnal, and R. K. Boncek, "Demonstration of all-optical Mach-Zehnder demultiplexer," Opt. Lett. **31**(9), 749–750 (1995).
7. T. Miyazaki and F. Kubota, "Simultaneous Demultiplexing and Clock Recovery for 160-Gb/s OTDM Signal Using a Symmetric Mach-Zehnder Switch in Electrooptic Feedback Loop," IEEE Photon. Technol. Lett. **15**(7), 1008–1010 (2003).
8. K.-Y. Wang, K. G. Petrillo, M. A. Foster, and A. C. Foster, "Ultralow-power all-optical processing of high-speed data signals in deposited silicon waveguides," Opt. Express **20**(22), 24600–24606 (2012).
9. T. D. Vo, H. Hu, M. Galili, E. Palushani, J. Xu, L. K. Oxenløwe, S. J. Madden, D.-Y. Choi, D. A. P. Bulla, M. D. Pelusi, J. Schröder, B. Luther-Davies, and B. J. Eggleton, "Photonic chip based transmitter optimization and receiver demultiplexing of a 1.28 Tbit/s OTDM signal," Opt. Express **18**(16), 17252–17261 (2010).
10. J. K. Fischer, R. Ludwig, L. Molle, C. Schmidt-Langhorst, A. Galperin, T. Richter, C. C. Leonhardt, A. Matiss, and C. Schubert, "High-speed digital coherent based on parallel optical sampling," J. Lightwave Technol. **29**(4), 378–385 (2011).
11. M. T. Kauffman, W. C. Banyai, A. A. Godil, and D. M. Bloom, "Time-to-frequency converter for measuring picosecond optical pulses," Appl. Phys. Lett. **64**(3), 270–272 (1994).

12. E. Palushani, H. C. Mulvad, M. Galili, H. Hu, L. K. Oxenløwe, A. T. Clausen, and P. Jeppesen, "OTDM-to-WDM Conversion Based on Time-to-Frequency Mapping by Time-Domain Optical Fourier Transformation," IEEE J. Sel. Top. Quantum Electron. **18**(2), 681–688 (2012).

13. H. C. H. Mulvad, E. Palushani, H. Hu, H. Ji, M. Lillieholm, M. Galili, A. T. Clausen, M. Pu, K. Yvind, J. M. Hvam, P. Jeppesen, and L. K. Oxenløwe, "Ultra-high-speed optical serial-to-parallel dataconversion by time-domain optical Fouriertransformation in a silicon nanowire," Opt. Exp. **19**(26), B825–B835 (2011).

14. E. Palushani, T. Richter, R. Ludwig, C. Schubert, H. C. H. Mulvad, A. T. Clausen, and L. K. Oxenløwe, "OTDM-to-WDM Conversion of Complex Modulation Formats by Time-Domain Optical Fourier Transformation," Proc. Opt. Fiber Commun. (OFC) 2012, paper OTh3H.2.

15. B. W. Buckley, A. M. Madni, and B. Jalali, "Coherent time-stretch transformation for real-time capture of wideband signals," Opt. Express **21**(18), 21618–21627 (2013).

16. Y. T. Mazurenko, S. E. Putilin, A. G. Spiro, A. G. Beliaev, V. E. Yashin, and S. A. Chizhov, "Ultrafast time-to-space conversion of phase by the method of spectral nonlinear optics," Opt. Lett. **21**(21), 1753–1755 (1996).

17. P. C. Sun, Y. T. Mazurenko, and Y. Fainman, "Femtosecond pulse imaging: ultrafast optical oscilloscope," J. Opt. Soc. Am. A **14**(5), 1159–1170 (1997).

18. A. M. Kan'an and A. M. Weiner, "Efficient time-to-space conversion of femtosecond optical pulses," J. Opt. Soc. Am. B **15**(3), 1242–1245 (1998).

19. D. M. Marom, D. Panasenko, P.-C. Sun, and Y. Fainman, "Linear and nonlinear operation of a time-to-space processor," J. Opt. Soc. Am. A **18**(2), 448–458 (2001).

20. D. M. Marom, D. Panasenko, P.-C. Sun, Y. T. Mazurenko, and Y. Fainman, "Real-time spatial–temporal signal processing with optical nonlinearities," IEEE J. Sel. Top. Quantum Electron. **7**(4), 683–693 (2001).

21. J.-H. Chung and A. M. Weiner, "Real-time detection of femtosecond optical pulse sequences via time-to-space conversion in the lightwave communications band," J. Lightwave Technol. **21**(12), 3323–3333 (2003).

22. A. M. Weiner, "Femtosecond pulse shaping using spatial light modulators," Rev. Sci. Instrum. **71**(5), 1929–1960 (2000).

23. D. Shayovitz and D. M. Marom, "High-resolution, background-free, time-to-space conversion by collinearly phase-matched sum-frequency generation," Opt. Lett. **36**(11), 1957–1959 (2011).

24. D. Shayovitz, H. Herrmann, W. Sohler, R. Ricken, C. Silberhorn, and D. M. Marom, "High resolution time-to-space conversion of sub-picosecond pulses at 1.55μm by non-degenerate SFG in PPLN crystal," Opt. Exp. **20**(24), 27388–27395 (2012).

25. D. Shayovitz, H. Herrmann, W. Sohler, R. Ricken, C. Silberhorn, and D. M. Marom, "Time-to-space conversion of ultrafast waveforms at 1.55 μm in a planar periodically poled lithium niobate waveguide," Opt. Lett. **38**(22), 4708–4711 (2013).

26. D. Shayovitz, H. Herrmann, W. Sohler, R. Ricken, C. Silberhorn, and D. M. Marom, "Full-field reconstruction of ultrashort waveforms by time to space conversion interferogram analysis," Opt. Express **22**(17), 20205–20213 (2014).

1. Introduction

The growth trend in global communications traffic shows no sign of slowing, whereas current optical communications networks based on wavelength division multiplexing (WDM) are nearing their available bandwidth limit [1]. In order to support continued growth it is increasingly necessary to exploit all available multiplexing and modulation degrees of freedom, such as polarization multiplexing and complex amplitude modulation. Advanced modulation formats such as quadrature phase shift keying (QPSK) together with coherent detection of the received signal may be employed. Indeed, recently deployed optical networks utilize polarization multiplexing and 2 bits-per-symbol modulation of an electronically generated 25 Gbaud/s serial channel to reach single-wavelength channel data rates of100 Gb/s. Another advantage of coherent detection is apparent when it is combined with digital signal processing (DSP). This enables electronic compensation of linear distortions such as chromatic dispersion and polarization mode dispersion, and some nonlinear distortions such as cross-phase modulation (XPM) and four-wave mixing (FWM),undergone by short pulses propagating in optical fiber [2].

Optical time division multiplexing enables high bit rate data transmission whilst lowering the number of wavelength channels, thereby minimizing the number of laser sources required and reducing overall system management complexity. By combining OTDM with complex amplitude modulation a single-wavelength channel can be generated at greater than 1 Tb/s [3], exceeding the highest modulation rates in the electronic domain which are limited by device physics to <100 GHz. An OTDM channel is typically produced by using passive optical delay lines to interleave pulses from multiple low baud rate tributaries into unique time slots on a frame-by-frame basis. OTDM demultiplexing is more challenging and several demultiplexing techniques have

been investigated. These include the nonlinear optical loop mirror [4, 5], XPM-based Mach-Zehnder switch [6, 7], FWM-based spectral filtering extraction [8, 9] and coherent detection by parallel optical sampling with a pulsed local oscillator [10]. All these methods however are limited to single bit extraction, with multiple devices needed to completely demultiplex the OTDM channel. Since the power consumption and overall complexity of the demultiplexing stage increase with each additional device, the scalability of these techniques to higher symbol rates is challenging. In addition the task of inter-device clock synchronisation, necessary in order to extract the correct tributary at each device, becomes difficult for higher bit rates.

Serial-to-parallel demultiplexing can overcome these problems by simultaneously extracting all the bits in an OTDM frame. With a single reference pulse performing the entire demultiplexing operation the problem of inter-device clock synchronization, as for single-bit extraction, becomes one of synchronizing the reference pulse to the several tens of picoseconds wide OTDM frame, a less onerous task. Serial-to-parallel demultiplexing has been successfully demonstrated by using time-to-frequency conversion, where the temporal pulse envelope is imprinted onto the spectrum of an FWM wave [11, 12]. Individual tributaries of the OTDM signal can be demultiplexed and then either direct detected [13] or coherently detected with a local oscillator (LO) tuned to the specific wavelength channel [14]. However if phase continuity between tributaries is required then the LO's for coherent detection have to be phase locked across the broad converted spectrum [15], making phase detection more difficult. We propose and demonstrate the time-to-space conversion technique for serial-to-parallel demultiplexing of a high bit rate OTDM channel, including recovery of phase information by coherent detection of the demultiplexed narrowband pulses with a single LO source.

Time-to-space conversion is an all-optical demultiplexing technique based on spectrally-resolved sum-frequency generation (SFG) between a signal pulse stream and a single reference pulse. It works by transferring the spectrally broadband time domain information of the signal pulses to a spatial image formed by quasi-monochromatic SFG light [16–21]. By combining the gating effect of SFG with spectral processing techniques developed originally for ultrashort pulse shaping [22], time-to-space conversion can demultiplex a high bit rate OTDM channel to multiple parallel spatial channels for direct detection by an array of photo receivers [21]. Alternatively, homodyne mixing of the quasi-monochromatic SFG light with a narrow linewidth local oscillator (LO) allows coherent detection of phase information, making demultiplexing by time-to-space conversion compatible with advanced modulation formats. We have previously demonstrated high resolution time-to-space conversion in bulk and slab waveguide nonlinear media [23–25], as well as phase measurements of time-to-space converted ultrashort waveforms by interferogram recording in the space domain [26]. Here we report real-time demultiplexing and single-shot coherent detection of phase-modulated sub-picosecond pulses at 1.55 μm. This result supports the potential of time-to-space conversion for high bit rate OTDM demultiplexing applications.

2. Time to space conversion principle of operation

The principle of time-to-space conversion [18–21] is shown in Fig. 1.The incoming OTDM signal bit stream and a single locally generated reference pulse, at non-degenerate central wavelengths, are given equal magnitude but opposite direction spatial dispersions by pairs of diffraction gratings and Fourier lenses. Their resolved spectra overlap in space at the Fourier plane, where a nonlinear $\chi^{(2)}$ crystal is located. SFG occurs between pairs of overlapping frequency components of the signal and reference spectra at each point in space. Due to the matched yet flipped spatial dispersions, each pair of overlapping frequency components adds up to the same sum-frequency. The result is aspatially coherent narrow bandwidth SFG wave generated along the entire crystal aperture, with automatic phase-matching across the bandwidth of the dispersed pulses. The temporal walk-off problem typically associated with ultrashort pulses in a dispersive nonlinear medium is negligible since the SFG interaction occurs between pairs of quasi-

monochromatic beamlets, each at different frequencies, at the Fourier plane of the time-to-space processor.
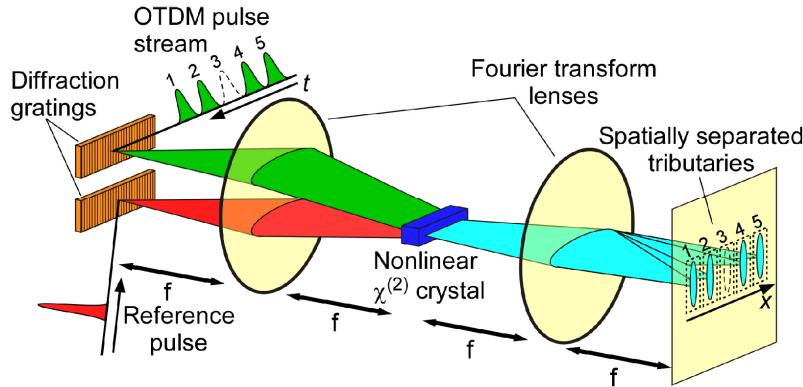

Fig. 1. Time-to-space conversion concept. Time domain information is converted to a spatial image with the temporal coordinate t mapped linearly to a spatial coordinate x. Note that in our experimental setup the signal and reference beams propagate collinearly in the nonlinear crystal, whereas here they are shown at crossed angles for clarity. The dashed line in the OTDM pulse stream represents an empty bit slot.

The time delay information between a signal pulse in the OTDM pulse stream and the reference pulse is carried by the spectral phase of the spatially dispersed waveforms, which is converted to a linear spatial phase on the generated SFG wave. A second Fourier lens after the nonlinear crystal coverts this linear phase on the quasi-monochromatic waveform to a transverse spatial shift of the focused pulse images at the output image plane. The result is a quasi-static spatial image of the signal pulse (assuming that the reference pulse has a much shorter temporal duration) [20]:

$$U_{out}(x,t) = w\left(-\frac{c(t-t_0)}{\alpha}\right) \cdot w\left(\frac{ct}{\alpha}\right) \cdot s\left(\frac{\alpha x}{c} - t_0\right) \otimes r\left(-\frac{\alpha x}{c}\right) \cdot \exp\left(-j(\omega_S + \omega_R)t\right)$$
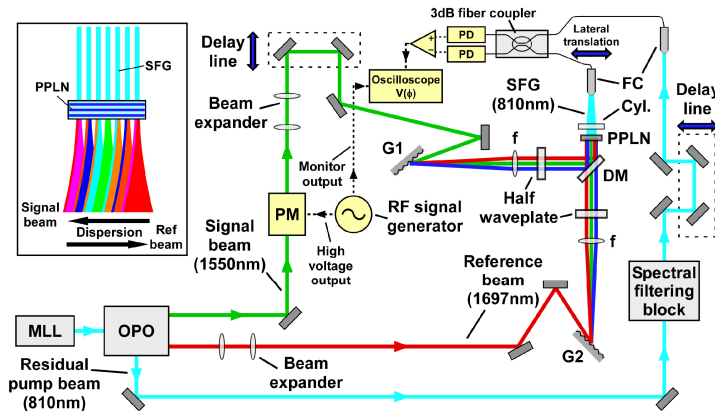
(1)

Fig. 2. Experimental setup for time-to-space conversion with coherent detection (MLL, mode-locked laser; OPO, optical parametric oscillator; PM, phase modulator; G1/G2, diffraction grating; f, Fourier lens; DM, dichroic mirror; Cyl., cylindrical lens; FC, fiber collimator; PD, photodetector). Note that the SFG beam fiber collimator can be laterally translated to detect different spatially demultiplexed pulse images. The spectral filtering block represents a diffraction grating – Fourier lens – spatial filter setup. A high voltage amplifier (not shown) was used to amplify the RF signal driving the phase modulator. Dashed lines represent electrical connections. Inset: dispersed signal and reference beams at the PPLN. No second harmonic components were generated for the signal and reference in the crystal due to phase matching bandwidth limitation of the PPLN.

where $s(\bullet)$ and $r(\bullet)$ are the functional forms of the signal and reference pulses, mapped to the output plane spatial coordinate x, $w(\bullet)$ is the beam aperture of the input waves forming the temporal aperture of the spectral processor, $\omega_{S,R}$ are the signal and reference pulse central angular frequencies respectively, α is the dispersion parameter, c is the speed of light, t_0 is the time delay of an individual signal pulse within the frame with respect to the reference pulse and $\otimes$ is the convolution operator. The use of signal and reference pulses at non-degenerate central wavelengths enables spectral bandpass filtering of the output light, in order to block background light arising from second harmonic generation by each of the input waves [23]. The space domain image consisting of separated beams can be directly detected [23–25] by an array of photodetectors, resulting in an instantaneous intensity measurement at each time slot within the OTDM frame. Whilst this would be sufficient for detecting an on-off keying (OOK) modulated bit stream, the phase information contained in the quasi-monochromatic SFG light is lost with intensity detection. Here we demonstrate coherent detection of the phase information by homodyne mixing of the SFG output light with a narrowband LO at a balanced detector.

3. Coherent detection time-to-space conversion experiment

Figure 2 shows our experimental setup. A mode-locked laser (MLL) generates ~100 fs bandwidth-limited pulses at 810 nm with an 80.2 MHz repetition rate. These are converted by an optical parametric oscillator (OPO) to 'signal' pulses at 1550 nm central wavelength (beam path shown in green) and 'reference' pulses at 1697 nm (shown in red). The signal pulse train is directed into an electro-optic phase modulator based on a bulk KTP crystal (New Focus 4064). The phase modulator is driven with a 500 kHz sinusoidally varying high voltage in order to apply positive and negative phase shifts of up to 1.5 radians to the signal pulses. A series of n signal pulses exiting the phase modulator then has the form:

$$s(t) = \sum_k p(t - kt_0) \exp(jf_{RF}t) \tag{2}$$

where $p(\bullet)$ is the temporal envelope of the signal pulse located at time kt_0 in the pulse train, k is an integer representing the pulse number, t_0 is the pulse-to-pulse time separation and f_{RF} is the phase modulation frequency. The modulated signal pulse then passes through a delay line in order to adjust its time delay with respect to the reference pulse on arrival at the time-to-space processor.

The signal pulse is then spatially dispersed by a diffraction grating and Fourier lens. At the same time the non-modulated reference pulse is given an equal but opposite spatial dispersion by another diffraction grating and Fourier lens. The two dispersed pulses are superimposed by a dichroic mirror and are incident on a periodically-poled lithium niobate (PPLN) nonlinear crystal located at the focal plane (see inset in Fig. 2). The PPLN crystal has a poling period of 20.3 μm and dimensions of 12 mm and 8 mm in the spatial dispersion direction and light propagation direction, respectively. The Rayleigh length of the focused signal and reference spectral components inside the PPLN was estimated as ~1 mm, by calculating the focused spectral component spot size from measurements of the spectral resolution and spatial dispersion of the light at the Fourier plane.

The signal and reference beams' average powers at the PPLN entrance face were measured as 134mW and 75mW respectively, resulting in pulse energies of 1.7nJ and 0.9nJ and peak powers of 35 W and 19 W respectively. The spatial extent of the dispersed beams was approximately 4 mm in the horizontal (spatial dispersion) direction and 12 μm in the vertical (focused) direction (both sizes are the $1/e^2$ radius). Ideally the reference pulse peak power would be much higher than that of the signal pulse; however this was not available from the OPO used in this experiment. The peak powers were calculated assuming that the dispersed signal and reference pulses at the Fourier plane were stretched through the time-to-space converter time window, which was measured as 48ps (FWHM). Phase-matched SFG at each point in space resulted in the generation of sum-

frequency light centered at 810 nm with a −3dB bandwidth of 0.1 nm; the spectrum is shown in Fig. 3 (blue line). The THz bandwidth input sub-picosecond pulses are thereby transferred to a narrowband output SFG wave with an approximately 50 GHz bandwidth, which is within the detection bandwidth of fast optoelectronic detectors. The SFG beam average power emerging from the PPLN was measured as 22 μW.

The elliptical SFG beam was collimated in the vertical direction by a cylindrical lens placed after the PPLN, resulting in a more circular beam profile. At the same time the LO beam was generated by spectral filtering of the mode-locked laser residual pump pulse at 810 nm, which exits from the OPO (beam path shown in cyan in Fig. 2). A diffraction grating, Fourier lens and narrow slit (represented by the 'spectral filtering block' in Fig. 2) were used to narrow the −3dB bandwidth of the residual pump pulse from approximately 9 nm to 0.1 nm to match the SFG spectrum; the LO spectrum is also shown in Fig. 3 (green line). Another delay line was used to obtain temporal overlap of the filtered LO pulse with the SFG pulse at
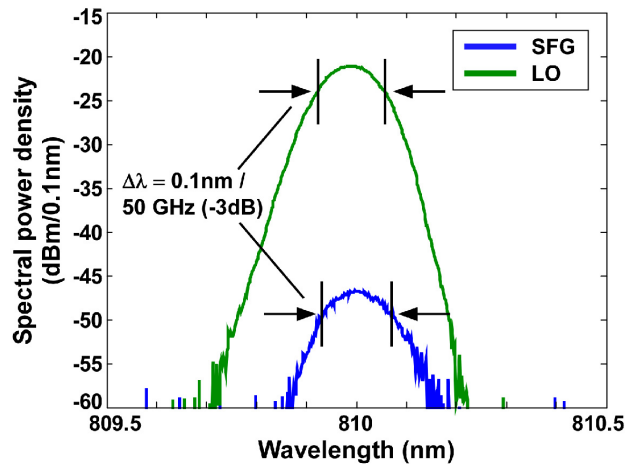

Fig. 3. Time-to-space converted SFG spectrum (blue) and local oscillator spectrum (green). Each spectrum is centered at 810 nm and has a −3dB bandwidth of approximately 0.1 nm (~50 GHz). The measurements were made by alternately coupling the SFG and LO light from one of the −3 dB fiber coupler outputs into an optical spectrum analyzer set to 0.1 nm resolution.

the balanced detector.

The SFG and LO beams were each coupled via fiber collimators into separate single mode fibers (at 810 nm). There was an approximately 9 dB insertion loss of the SFG light into its fiber collimator, due to mode mismatch between the SFG beam and the collimator mode. The SFG and LO light was then mixed in a −3 dB coupler, obtaining different beat measurements at the two output ports of the coupler. The light from each output was then incident on the positive and negative photodiodes of a 350 MHz bandwidth silicon balanced detector (Thorlabs PDB430A-AC). Interference between the SFG and LO light converted the SFG phase modulation into intensity modulation which could be registered by the photodiodes. The SFG and LO optical powers arriving at the balanced detector were individually measured as 0.003 mW and 5 mW respectively. By equalizing the optical power incident on each photodiode the DC component of the summed photocurrents was minimized, leaving the RF sum component whose amplitude was proportional to the SFG and LO optical power and, crucially, to the relative phase between the SFG and LO.

The RF electrical signal was recorded on a 12 GHz oscilloscope (Agilent DSO 81204A) and an exemplary trace is shown in Fig. 4(a), along with the phase modulator driving signal. A sinusoidal modulation of the SFG pulse train with modulation frequency 500 kHz can also be seen. However, as is evident in Fig. 4(a) and Fig. 4(b), an electrical signal was present at the balanced photodetector RF output even for zero overall phase of

the homodyne mixing product. We believe this was due to ringing effects caused by the limited bandwidth of the photodiodes and transimpedance amplifier in the balanced photodetector. Figures 4(b), 4(c) and 4(d) show close-ups of individual pulses taken from the trace in Fig. 4(a) at zero, $\pi/2$ and $3\pi/2$ phases of the sinusoidal driving signal. Figures (c) and (d) provide clear evidence for single-shot coherent detection of negatively and positively phase modulated pulses respectively. A small phase shift between the phase modulator driving signal and the response of the modulated signal as measured on the oscilloscope is also apparent; this is due to the constant phase offset between on the LO wave with respect to the signal. In coherent reception, this phase offset is eliminated by an estimation and DSP.
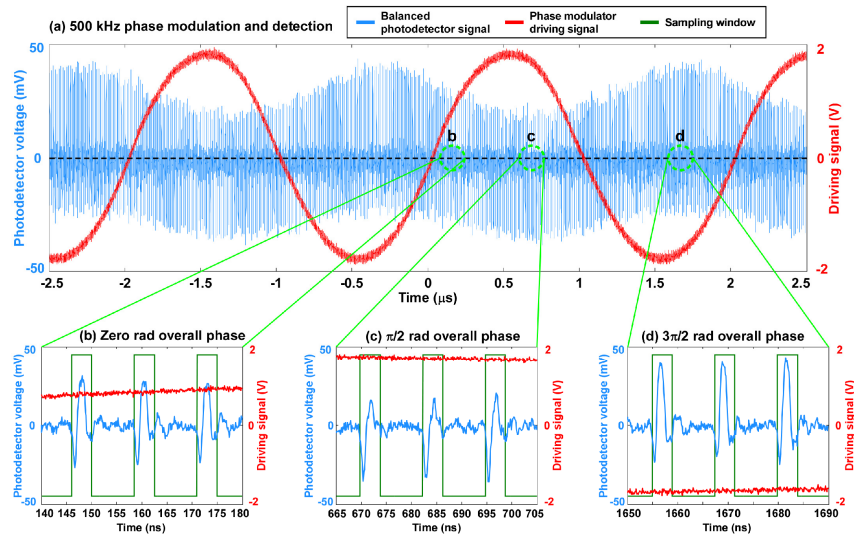

Fig. 4. Coherent detection of time-to-space converted phase modulated pulses. (a) Oscilloscope trace showing the balanced photodetector signal (blue) and the 500 kHz sinusoidal driving signal applied to the phase modulator (red). The phase modulator driving signal shown was taken from the monitor output of the high voltage amplifier which was used to drive the phase modulator. (b), (c)and (d) Close-ups of individual pulses detected at various phases (note the nanosecond time scale).The sampling windows used to derive the data shown in Fig. 5 are represented by green rectangles; the window amplitude varies from zero to one in a square wave fashion. The location on the oscilloscope trace of each close-up is indicated by a green dashed circle in (a).The waveforms seen in (b) are due to ringing by the 350 MHz bandwidth balanced detector, which degrades the quality of the phase-demodulated signal as can be seen in (a). However negative and positive demodulated pulses can clearly be seen in (c) and (d) respectively. Note that due to a residual fixed phase on the LO, there is an offset between the phase modulator driving signal phase and the phase of the received signal.

To obtain a clearer phase-demodulated output signal, the oscilloscope trace shown in Fig. 4(a) was processed to extract the signal component only. The signal was extracted by integrating over a time window matched to the detector response time and timed to collect the signal energy; the time windows are illustrated by the green rectangles in Figs. 4(b), 4(c) and 4(d).The width of each time window is set to 4 ns to collect the energy over the whole electrical waveform generated by each detected pulse. The electrical signal present within each window results in a single average voltage value for each detected pulse, i.e. the extracted measured value per pulse as expected in a conventional receiver; these are plotted as magenta

(a) Window-sampled and averaged photodetector signal

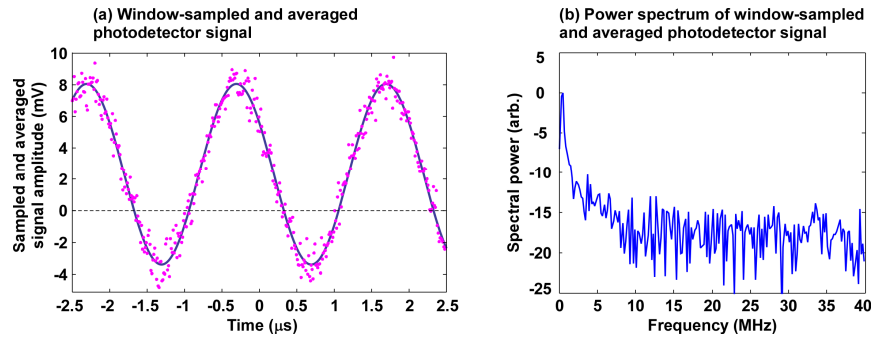**(b) Power spectrum of window-sampled and averaged photodetector signal**

Fig. 5. Time window sampled and averaged photodetector signal. (a) Time domain representation showing the average photovoltage for each pulse (magenta dots) with a sine curve fit to the data points (blue line). (b) Frequency domain representation of the sampled signal, found by taking the Fourier transform of the photovoltage data points in (a). Peak at 500 KHz modulation apparent.

dots in Fig. 5(a).

In order to determine the signal to noise ration (SNR) of the demodulated signal, a sine function was fitted to the sampled data points; this is shown as the blue line in Fig. 5(a). The fit resulted in a root mean squared amplitude and standard deviation of $v_{opt} = 4$ mV and $\sigma_v = 0.68$ mV respectively, giving an SNR of $v_{opt}^2 / \sigma_v^2 = 34$. We confirmed the noise level is the roughly the same when the LO is introduced alone (note the LO is three orders of magnitude more intense than the signal), as well as when there is no input optical signal, hence the noise is thermal in origin, whether originating from the balanced photodetector or more likely from the high speed real-time scope. Note that the signal modulation depth was limited to ~0.5 due to the maximum 1.5 radians phase modulation applied by the free-space phase modulator; this was in turn restricted by the highest driving voltage ($\pm$ 200 V) which could be supplied. Had full phase modulation depth been achieved (π radians of phase shift), the SNR would quadruple to 136 since the noise figure would be expected to remain the same. Additionally, the 9 dB insertion loss of the SFG light into the fiber collimator further limited the signal level at the receiver. Eliminating this loss would result in an approximately factor 3 increase in signal amplitude, thus giving an additional factor 9 increase in SNR. Therefore under ideal conditions an SNR beyond 1000 could potentially be achieved. The power spectrum of the sampled signal, found by taking the Fourier transform of the data points shown in Fig. 5(a), is shown in Fig. 5(b); a peak due to the applied phase modulation can be seen at 500 kHz.

4. Conclusions

In conclusion we have demonstrated real-time demultiplexing to the spatial domain and single-shot coherent detection of a phase modulated ultrashort pulse train by time-to-space conversion. The inherently narrow linewidth SFG output signal of the time-to-space conversion process enables interferometric detection of phase information originally encoded on ultrashort pulses. This demonstration underlines the potential of time-to-space conversion as an all-optical serial-to-parallel demultiplexer capable of transferring wideband time domain signals to a slowly varying spatial domain image. By bridging the optical-electrical bandwidth gap, time-to-space conversion can be a valuable tool in support of ultrahigh bit rate OTDM optical communications.